AGU100 ADVANCING EARTH AND SPACE SCIENCE

Geophysical Research Letters

RESEARCH LETTER

10.1029/2018GL077794

Global Contributions of Incoming Radiation and Land Surface Conditions to Maximum Near-Surface Air Temperature Variability and Trend

Clemens Schwingshackl[1], **Martin Hirschi**[1], **and Sonia I. Seneviratne**[1]

[1] Institute for Atmospheric and Climate Science, ETH Zürich, Zürich, Switzerland

Key Points:

- The used linear regression model explains about 79% of interannual temperature variability and 99% of multidecadal temperature trend
- Radiation explains on average about 75% to 85% of the total explained variance, while land surface conditions contribute about 15% to 25%
- Radiation is essential for explaining temperature variability almost everywhere, land surface conditions in some confined regions

Supporting Information:

- Supporting Information S1

Correspondence to:
C. Schwingshackl,
clemens.schwingshackl@env.ethz.ch

Citation:
Schwingshackl, C., Hirschi, M., & Seneviratne, S. I. (2018). Global contributions of incoming radiation and land surface conditions to maximum near-surface air temperature variability and trend. *Geophysical Research Letters*, *45*, 5034–5044. https://doi.org/10.1029/2018GL077794

Received 5 OCT 2017
Accepted 2 MAY 2018
Accepted article online 14 MAY 2018
Published online 20 MAY 2018

Abstract The evolution of near-surface air temperature is influenced by various dynamical, radiative, and surface-atmosphere exchange processes whose contributions are still not completely quantified. Applying stepwise multiple linear regression to Coupled Model Intercomparison Project phase 5 (CMIP5) model simulations and focusing on radiation (diagnosed by incoming shortwave and incoming longwave radiation) and land surface conditions (diagnosed by soil moisture and albedo) about 79% of the interannual variability and 99% of the multidecadal trend of monthly mean daily maximum temperature over land can be explained. The linear model captures well the temperature variability in middle-to-high latitudes and in regions close to the equator, whereas its explanatory potential is limited in deserts. While radiation is an essential explanatory variable over almost all of the analyzed domain, land surface conditions show a pronounced relation to temperature in some confined regions. These findings highlight that considering local-to-regional processes is crucial for correctly assessing interannual temperature variability and future temperature trends.

Plain Language Summary The evolution of near-surface air temperature is mostly impacted by radiation, heat advection, and land-atmosphere interactions. In this study, we quantify the impact of incoming shortwave and longwave radiation as well as soil moisture and albedo on year-to-year variability and long-term trends of average daily maximum temperature. Applying a linear regression model to the output of climate models, about 80% of the year-to-year temperature variability and 99% of the long-term temperature trend can be explained by the four considered radiation and land surface variables. The radiation components are essential for explaining the temperature evolution almost everywhere. Soil moisture and albedo impact temperature in some confined regions. Incoming longwave radiation contributes strongly to year-to-year variability in high latitudes and explains most of the long-term temperature trend. Incoming shortwave radiation is important in the tropics and in middle-to-high latitude during winter. Albedo is of special importance in regions that experience varying snow cover in different years or snow cover changes with climate change. The impact of soil moisture is highest in regions, where it limits the amount of evapotranspiration. The results highlight the fact that local-to-regional processes are relevant both for year-to-year temperature variability and future temperature trends.

1. Introduction

Near-surface air temperature is one of the most direct experiences of weather and climate for people in their everyday life. Its short-term variability and long-term trend are thus among the most investigated topics in climate research (e.g., Ji et al., 2014; Jones, 1999; Jones et al., 2012; Legates & Willmott, 1990). Due to its location close to the interface between land/ocean and the atmosphere, the near-surface air is impacted by various exchange processes between these three Earth system compartments.

One of the most important factors determining near-surface air temperature is the amount of incoming radiation at the surface. On land, the absorbed net radiation as well as its partitioning into the different heat fluxes is further modulated by the state of the land surface. Here we quantify the contributions of both incoming radiation as well as land surface conditions to interannual variability and multidecadal trend of monthly means of daily maximum near-surface air temperature. In particular, incoming shortwave radiation, incoming longwave radiation, soil moisture, and albedo are considered as potential drivers.

Incoming (solar) shortwave radiation constitutes the largest energy input to the climate system. Variations of incoming shortwave radiation (e.g., due to changing incident angle, cloud cover, or aerosol effects) are thus an important source of temperature variability and also contribute to temperature trends (e.g., Budyko, 1969; Lohmann & Feichter, 2005; Reitan, 1974).

Incoming longwave radiation bears information about the amount of outgoing thermal radiation from the Earth's surface that is absorbed and re-emitted in the atmosphere. It depends on atmospheric conditions, such as cloud cover (e.g., Stephens & Webster, 1981), water vapor (Compo & Sardeshmukh, 2009), or greenhouse gas concentrations (Arrhenius, 1896) and includes thus both short-term weather and long-term climate effects (Philipona et al., 2005; Pithan & Mauritsen, 2014).

The albedo determines how much of the incoming shortwave radiation is reflected back to space. It has a particularly pronounced impact on temperature in regions that experience transitions between snow-covered and snow-free states over the course of the year (Ellis & Leathers, 1999). Changes in albedo caused by global warming can have important impacts locally (e.g., polar amplification; Graversen & Wang, 2009; Pithan & Mauritsen, 2014) and also in more extended regions (Hall, 2004).

Soil moisture influences the partitioning of net radiation into sensible and latent heat fluxes and thus impacts near-surface air temperature in various regions of the world (e.g., Miralles et al., 2012; Schwingshackl et al., 2017; Seneviratne et al., 2010) especially during summer (Fischer et al., 2012; Lenderink et al., 2007; Seneviratne et al., 2006).

Furthermore, dynamical processes in the atmosphere—like large-scale circulation (Jones, 1999; Xoplaki et al., 2003) and the sequence of low-/high-pressure systems (e.g., Rodrigues & Woollings, 2017; Sillmann & Croci-Maspoli, 2009)—that lead to a geographical redistribution of energy impact near-surface air temperatures. In several regions, about half of the near-surface air temperature variability on monthly time scales can be explained by thermal advection (Holmes et al., 2016).

On longer time scales, atmospheric greenhouse gas concentrations (Intergovernmental Panel on Climate Change, 2013), sea surface temperatures (Hoerling et al., 2008), and climate oscillations (Chylek et al., 2016; Schleussner et al., 2014; Stolpe et al., 2017) contribute to temperature variability and trends by influencing the above-mentioned immediate drivers. For example, expressing local near-surface air temperature as a linear function of global mean temperature, over 90% of the local multidecadal temperature trend can be explained (Sutton et al., 2015).

Here we apply multiple linear regression (MLR) to quantify the contributions of incoming radiation and land surface conditions on temperature variability and trend. Additionally, we estimate the influence of thermal advection. As we are particularly interested in the contributions of land surface conditions to the temperature evolution, we focus on monthly mean daily maximum temperature for which the influence of soil moisture is especially pronounced (Jaeger & Seneviratne, 2011). Using a linear approximation, as we do here, is generally a simplification of reality. One needs thus to keep in mind the nonlinear nature of the Earth system (Good et al., 2015) and interpret the results cautiously.

2. Methods and Data

2.1. Multiple Linear Regression

As a generalization of linear regression, MLR is often used to describe the relationship between a set of dependent variables and multiple explanatory variables (Neter et al., 2004). However, adding more explanatory variables to MLR leads to a higher fraction of explained variance merely due to the increased degrees of freedom ("overfitting"). Thus, the number of explanatory variables has to be limited. This can be achieved by using special fitting tools, such as stepwise multiple linear regression (e.g., Hocking, 1976). This algorithm successively adds (removes) explanatory variables to (from) the model and decides whether to include the explanatory variable based on the p value (obtained from the F statistic) of the model with and without the respective variable. Here we use stepwise regression with forward selection, that is, starting with no variables and adding them successively in ascending order of their p values (up to the maximum p value of 0.05). Regression coefficients that are not included in the final model (due to the stepwise MLR selection procedure) are set to zero. Uncertainty estimates of the stepwise MLR results are calculated using jackknife resampling (e.g., Efron, 1982). Additionally, we apply least absolute shrinkage and selection operator (LASSO) regression (Tibshirani, 1996) to test the robustness of the results.

2.2. Partial and Semipartial Correlation

A standard metric to rate the relative importance of explanatory variables is the Pearson correlation coefficient, whose square (the coefficient of determination R^2) measures the amount of total variability accounted for by each explanatory variable without considering the others. Closely related to the Pearson correlation coefficient is the partial correlation coefficient $\rho_{XY \cdot \mathbf{Z}}$ (e.g., Brown & Hendrix, 2005), which measures the degree of correlation between two variables (X, Y), controlling for a set of other variables ($\mathbf{Z}$). The squared partial correlation coefficient, $\rho^2_{XY \cdot \mathbf{Z}}$, can be interpreted as how much of the remaining unexplained variance of Y is explained by the nth variable X after the introduction of $n-1$ variables $\mathbf{Z}$.

The squared semipartial correlation coefficient measures the increase in R^2 from adding one explanatory variable (Velicer, 1978). For independent explanatory variables the squared semipartial correlation coefficients add up to R^2. If explanatory variables are correlated, this does not hold anymore. For this case, Azen and Budescu (2003) propose to estimate the additional contribution of an explanatory variable by estimating the average R^2 increase of adding the variable to all regression models that contain a subset of the other explaining variables. For n explanatory variables one obtains 2^{n-1} semipartial correlation estimates for each variable, which are averaged. Azen and Budescu (2003) propose a special averaging method that conserves additivity, so that the sum of all squared semipartial correlations adds up to R^2. Moreover, the variation of the squared semipartial correlations constitutes a proxy for the collinearities between the explanatory variables and can serve as a form of uncertainty estimation.

2.3. Data

The analysis is based on the output of 35 Coupled Model Intercomparison Project phase 5 (CMIP5) models (Taylor et al., 2012, see supporting information Table S1 for an overview) using historical simulations and future scenarios under the Representative Concentration Pathway 8.5 (Riahi et al., 2011). The calculations are conducted on each grid point individually, after performing a bilinear interpolation to a common 2.5° grid.

Monthly mean values of daily maximum near-surface air temperature (based on daily maximum 2 m air temperature, T), incoming shortwave radiation at the surface (R_{sd}), incoming longwave radiation at the surface (R_{ld}), soil moisture (θ), and land albedo (α) are used for the analysis. The data are averaged separately for austral (December-January-February) and boreal summer (June-July-August), yielding one value per season, grid box, and year for each variable. Since albedo is not well defined when incoming shortwave radiation is zero, regions that experience polar nights are masked in the respective winter hemisphere.

Two different time spans are considered in the analysis: 1970–1999 to analyze the contribution of the single explanatory variables to interannual temperature variability and 1970–2099 to calculate their contribution to multidecadal temperature trends. To strictly separate these two effects from one another, and to correct for artificial increases of temperature variability (Scherrer et al., 2005), all variables used for the 30-year time span are linearly detrended, while the data for the 130-year span are grouped into thirteen 10-year long bins and averaged in each bin separately to eliminate the influence of year-to-year variability.

To overcome the issue that soil moisture values from different climate models are often not directly comparable (Koster et al., 2009), they can be standardized based on the variability in a defined base period (Berg et al., 2017). Here this approach is applied to all explanatory variables (R_{sd}, R_{ld}, θ, α), which are normalized by the standard deviation of all monthly values in the base period 1970–1999 on each grid box separately. The values of the dependent variable T are not transformed.

3. Results

3.1. Contributions of Radiation and Land Surface Conditions

3.1.1. Partial Correlation

Figure 1 shows the multimodel mean partial correlation between near-surface air temperature T and the different explanatory variables during the detrended time span 1970–1999 (i.e., interannual variability). Incoming shortwave and longwave radiation show overall the strongest partial correlations with temperature, with most climate models having significant correlations (indicated as gray/black stippling) in large areas of the world. Incoming shortwave radiation exhibits a pronounced change in correlations between JJA and DJF in middle-to-high latitudes, with high values during summer and low values during winter. In lower latitudes the patterns are similar in both seasons. Incoming longwave radiation has high partial correlations in middle-to-high latitudes in both seasons with slightly higher values during winter. For soil moisture

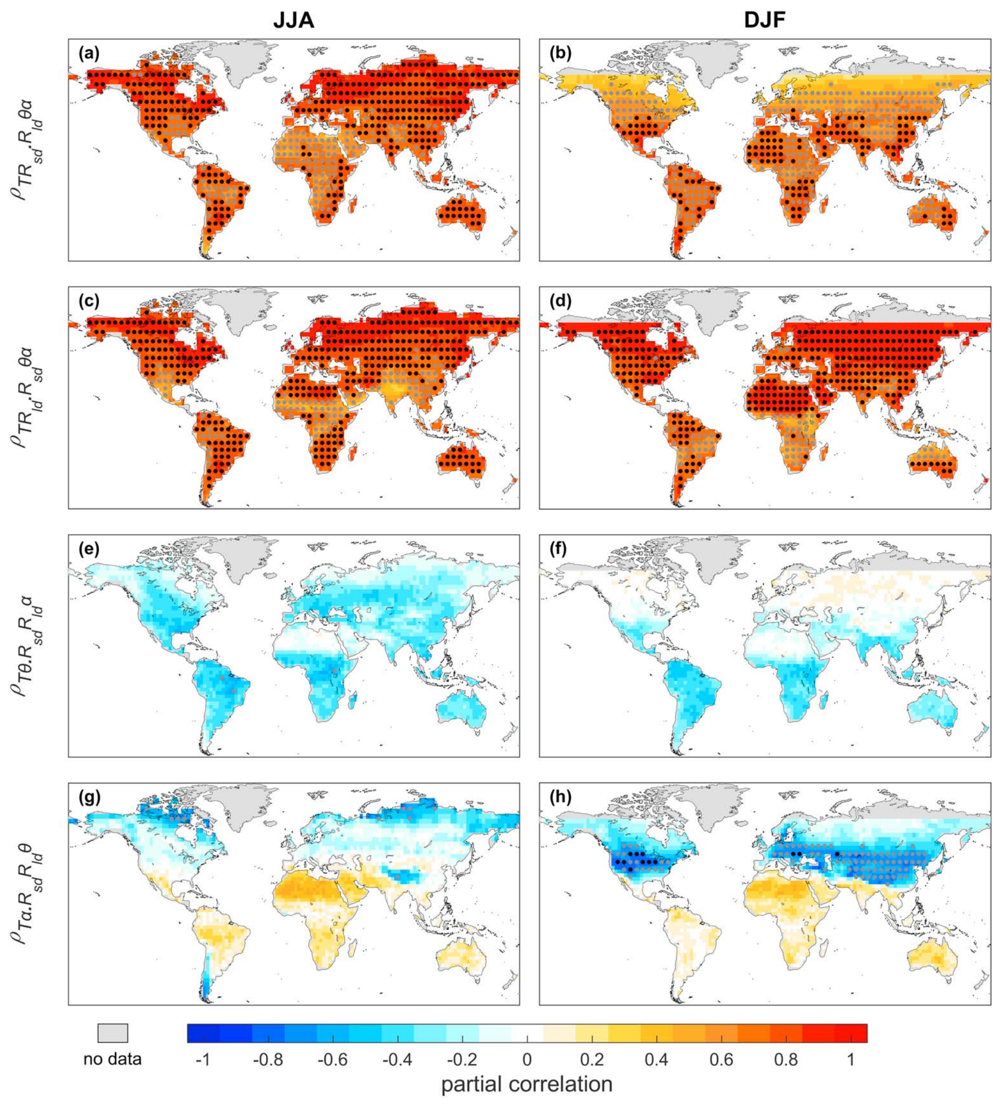

Figure 1. Multimodel mean partial correlation between near-surface air temperature T and (a, b) incoming shortwave radiation R_{sd}, (c, d) incoming longwave radiation R_{ld}, (e, f) soil moisture θ, and (g, h) albedo α controlling for all remaining explanatory variables. (left column) June-July-August (JJA) and (right column) December-January-February (DJF) during the detrended time span 1970–1999 (representing interannual temperature variability). Black (gray) dots indicate grid boxes where at least 90% (66%) of the climate models show significant correlations at the 5% level (significance levels were adapted according to Wilks, 2016).

and albedo the multimodel agreement is generally lower than for incoming radiation (indicated by the smaller stippling extent). Soil moisture exhibits negative correlations with temperature in many regions, except for deserts and large parts of the Northern Hemisphere during winter where they are close to zero. The correlations between albedo and temperature are negative in middle-to-high latitudes (especially during winter) and positive in large parts of the tropics.

The partial correlations for the multidecadal temperature trend (1970–2099, see supporting information Figure S1) are similar to those in Figure 1, with the difference that incoming longwave radiation has correlations close to unity almost all over the globe.

3.1.2. Stepwise MLR

The multimodel mean R^2 of the stepwise MLR for interannual temperature variability (i.e., for the detrended time span 1970–1999) is shown in Figures 2a and 2b. Averaged over the globe (weighted by latitude), R^2 is about 0.78 during boreal summer (JJA) and 0.79 during austral summer (DJF), indicating that more than three quarters of the interannual temperature variability can be explained by the linear model. Especially in high

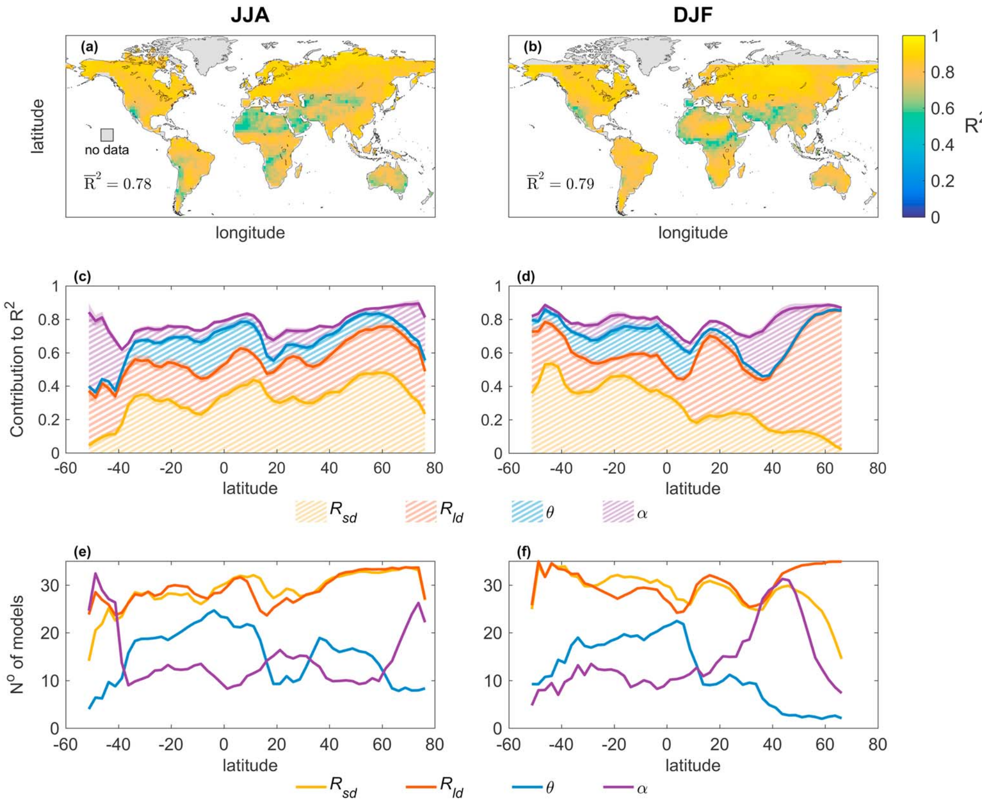

Figure 2. (a, b) Multimodel mean R^2 of the stepwise multiple linear regression for the detrended time span 1970–1999 (representing interannual temperature variability), (c, d) latitudinal mean (land only) contribution of the explanatory variables (striped areas) to total R^2 quantified by semipartial correlation, and (e, f) number of climate models for which stepwise multiple linear regression selected the respective explanatory variables. (left column) June-July-August (JJA) and (right column) December-January-February (DJF). Shading in Figures 2c and 2d indicates the uncertainty in the contribution of each explanatory variable to total R^2 and may be indicative of the collinearity between the variables.

latitudes and close to the equator, the linear model performs very well, while R^2 values are lower in dry areas. The results are consistent when applying LASSO regression (not shown).

Figures 2c and 2d display the latitudinal mean (land only) contribution of each explanatory variable (indicated as striped area) to R^2, estimated by the mean squared semipartial correlations. The sum of all contributions adds up to R^2. Incoming longwave radiation has the highest contribution (∼0.30 on average), followed by incoming shortwave radiation (∼0.29). The contribution of longwave radiation is more or less stable over the different latitudes but especially strong in winter in high latitudes. In contrast, shortwave radiation has the highest contribution in the respective summer hemisphere. The contributions of soil moisture (∼0.09) and albedo (∼0.11) are lower than those of radiation but important in some latitudes. Soil moisture shows the highest values between −40°S and 20°N, extending a bit further into the respective summer hemisphere, but decreasing strongly toward the poles. Albedo has the highest share in latitudes between 30° and 60° in the respective winter hemisphere and in high northern latitudes during JJA.

The variable selection of stepwise MLR is shown in Figures 2e and 2f. They display the latitudinal variations of the number of climate models for which the stepwise MLR includes the respective explanatory variables. Both incoming longwave and shortwave radiation are considered as significant variables for almost all climate models independent of the latitude (only in high latitudes their importance decreases). Soil moisture is a significant variable for most climate models around the equator and in midlatitudes in the Southern Hemisphere as well as in midlatitudes in the north during JJA. Albedo is significant for the majority of climate models in midlatitudes in the respective winter hemisphere and in very high latitudes in the north during JJA. Overall, the number of climate models in which each variable is considered as significant based on the stepwise MLR reflects their respective contributions to total R^2 as displayed in Figures 2c and 2d.

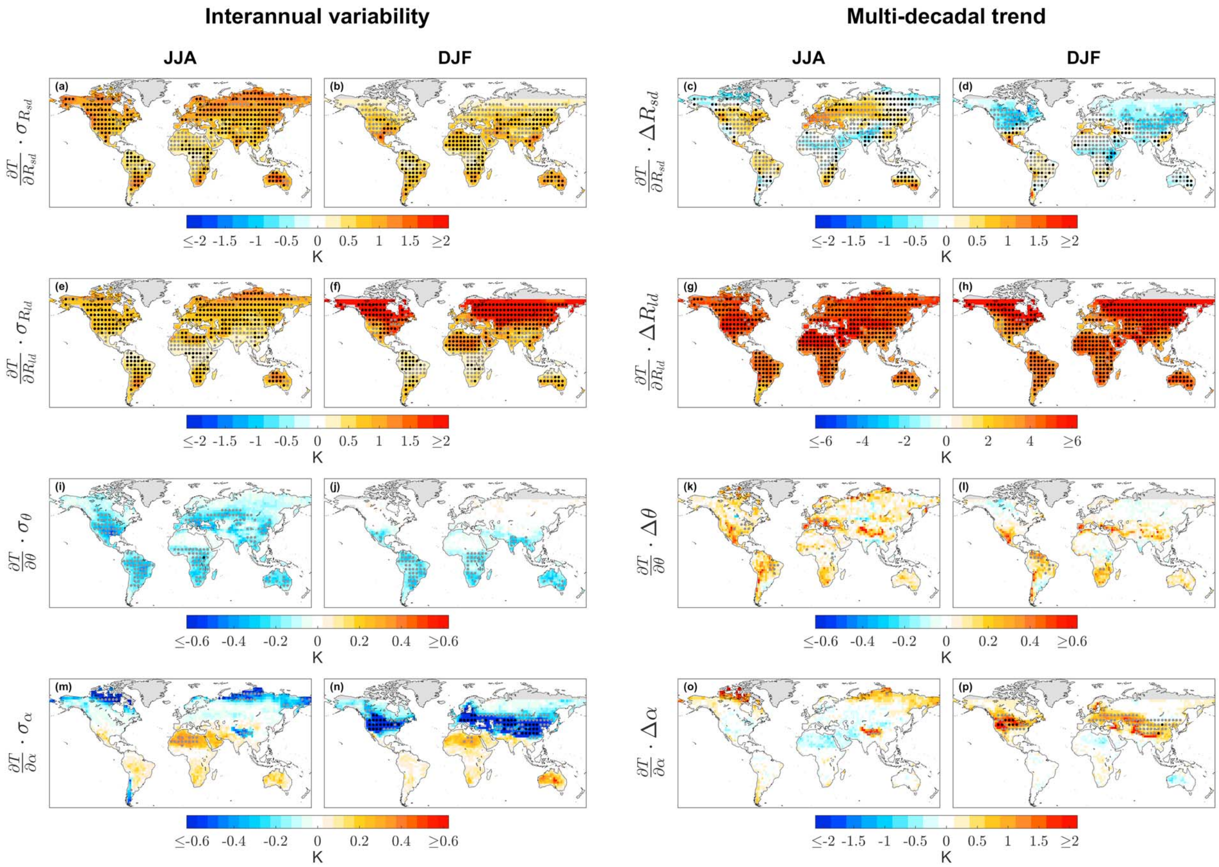

Figure 3. As in Figure 1 but for the multimodel mean contribution of (a–d) incoming shortwave radiation R_{sd}, (e–h) incoming longwave radiation R_{ld}, (i–l) soil moisture θ, and (m–p) albedo α to (left columns) interannual temperature variability in the detrended time span 1970–1999 and (right columns) the multidecadal temperature trend 1970–2099. Results are shown for June-July-August (JJA) and December-January-February (DJF). The contributions are calculated from the standard deviation σ_{x_i} of each variable (based on all linearly detrended monthly values in 1970–1999) for interannual variability and the mean change Δx_i between 1970–1999 and 2070–2099 for the multidecadal trend combined with the respective regression coefficients. Black (gray) dots indicate grid boxes where at least 90% (66%) of the models agree in sign with the multimodel mean. Note the different colorbar limits.

For the multidecadal temperature trend (1970–2099), the stepwise MLR yields very uniform R^2 values close to unity (supporting information Figure S2). Note that the sample size for the multidecadal trend is smaller than for interannual variability (13 data points instead of 30). While the contributions of the radiation components to R^2 exhibit less latitudinal variations compared to the results for interannual variability, the contribution patterns of land surface conditions stay overall similar (Figures S2c–S2f). Incoming longwave radiation contributes the largest part to R^2, followed by incoming shortwave radiation, albedo, and soil moisture. Although the importance of longwave radiation (which includes greenhouse gas and water vapor effects) is dominant, the other considered variables contribute a substantial part for explaining the multidecadal temperature trend as well. This highlights the fact that regional processes (and not only greenhouse gas concentration trends) are important to assess changes in near-surface air temperature (e.g., Berg et al., 2017; Intergovernmental Panel on Climate Change, 2013; Seneviratne et al., 2016).

3.2. Temperature Effect

3.2.1. Interannual Temperature Variability

The effect of typical variations of the four explanatory variables on temperature for JJA and DJF during the detrended time span 1970–1999 (i.e., for interannual temperature variability) is displayed in the left columns in Figure 3. Variations of incoming shortwave radiation have a strong impact on temperature in middle-to-high latitudes during summer (up to about 1.5 K) but only a minor contribution during winter. Close to the equator the influence of shortwave radiation is generally rather low. The impact of incoming longwave radiation on temperature is especially pronounced in middle-to-high latitudes during DJF. In lower latitudes and during JJA the influence is less strong but still ranges up to about 1.0 K. The impact of soil moisture variations on temperature is in general negative. It ranges up to about 0.5 K in some soil moisture hot spots (cf. Miralles et al., 2012; Schwingshackl et al., 2017), but it is negligible in deserts where water is scarce and in middle-to-high latitudes during winter when the soil is frozen. The impact of albedo variations is as well mostly negative. It is particularly strong in some regions in northern Canada, Siberia, the Tibetan Plateau, and Patagonia during JJA and in a band spanning from North America over Europe and Central Asia during DJF. In some desert regions albedo is positively related to temperature.

3.2.2. Multidecadal Temperature Trend

The contribution of changes in the explanatory variables (i.e., mean changes between 1970–1999 and 2070–2099) to the multidecadal temperature trend (1970–2099) is displayed in the right columns of Figure 3. Incoming longwave radiation (which includes greenhouse gas and water vapor effects) has by far the strongest (and always positive) effect on temperatures over land, especially pronounced in high northern latitudes during DJF. Incoming shortwave radiation contributes to temperature increases in Europe and large parts of Eurasia and North America during JJA, while it has a cooling effect in North America and Eurasia during winter. Moreover, it exhibits a dipole warming/cooling pattern in Australia and South America. Soil moisture trends also generally contribute to temperature increases, especially in the Mediterranean, the Southern USA/Mexico, and to a lesser magnitude in Brazil and South Africa. Albedo has a strong positive effect on temperature during DJF in parts of North America, Europe, and Central Asia, and in high northern latitudes during JJA. In contrast, albedo shows a slightly negative relation to the temperature evolution in deserts.

While for the radiation components most of the models agree on the sign of the change (indicated by the stippling), the results for the land surface conditions are more uncertain. Although climate models generally predict a positive relation between land surface conditions and the multidecadal temperature trend, the impact is not significant in the majority of models for most regions (see supporting information Figure S3).

4. Discussion

4.1. Impact of Other Drivers

Focusing on incoming radiation and land surface conditions as explaining variables, most of the interannual temperature variability and multidecadal temperature trend can be explained. Nevertheless, other variables may influence temperature as well. Holmes et al. (2016) showed that thermal advection can play an important role for month-to-month temperature variations. When we use only thermal advection as explanatory variable for the stepwise MLR, the obtained patterns and R^2 values are similar to the results of Holmes et al. (2016; see supporting information Figure S4). However, when thermal advection is included in combination with the other explanatory variables considered here, it only slightly improves R^2 (see supporting information Figures S5 and S6). This indicates strong collinearities between thermal advection and the other explanatory variables (compare Figures 2 and S5). Thermal advection can, for example, trigger albedo and soil moisture feedbacks that itself affect near-surface air temperature. Likewise, advection can alternate cloud cover and the amount of incoming shortwave radiation. If these confounding effects are not considered, the effect of thermal advection on temperature might thus be overestimated. On the other hand, thermal advection influences the amount of outgoing (and thus also incoming) longwave radiation. In regions with substantial thermal advection (see, e.g., Holmes et al., 2016), our study might thus overestimate the contribution of incoming longwave radiation to R^2 and underestimate the importance of thermal advection.

To test the impact of the mutual dependence between incoming longwave radiation and temperature for the multidecadal time scale, we replace incoming longwave radiation by global mean temperature, which also accounts for the climate change signal (Figure 4). While this replacement clearly has an impact on the sign and magnitude of incoming shortwave radiation (caused by the fact that shortwave radiation partly takes up the effect of longwave radiation, which acts as a hidden variable), the patterns of the land surface conditions stay generally the same (except for middle-to-high latitudes during DJF).

Another process influencing near-surface air temperatures is heat entrainment caused by the growth of the atmospheric boundary layer. It is especially important under convective conditions and can get particularly strong during heat waves (Miralles et al., 2014). On longer time scales, near-surface air temperature and its drivers, such as the ones considered here, can additionally be impacted by climate oscillations (Schleussner et al., 2014; Stolpe et al., 2017) and sea surface temperatures (Hoerling et al., 2008; Orth & Seneviratne, 2017).

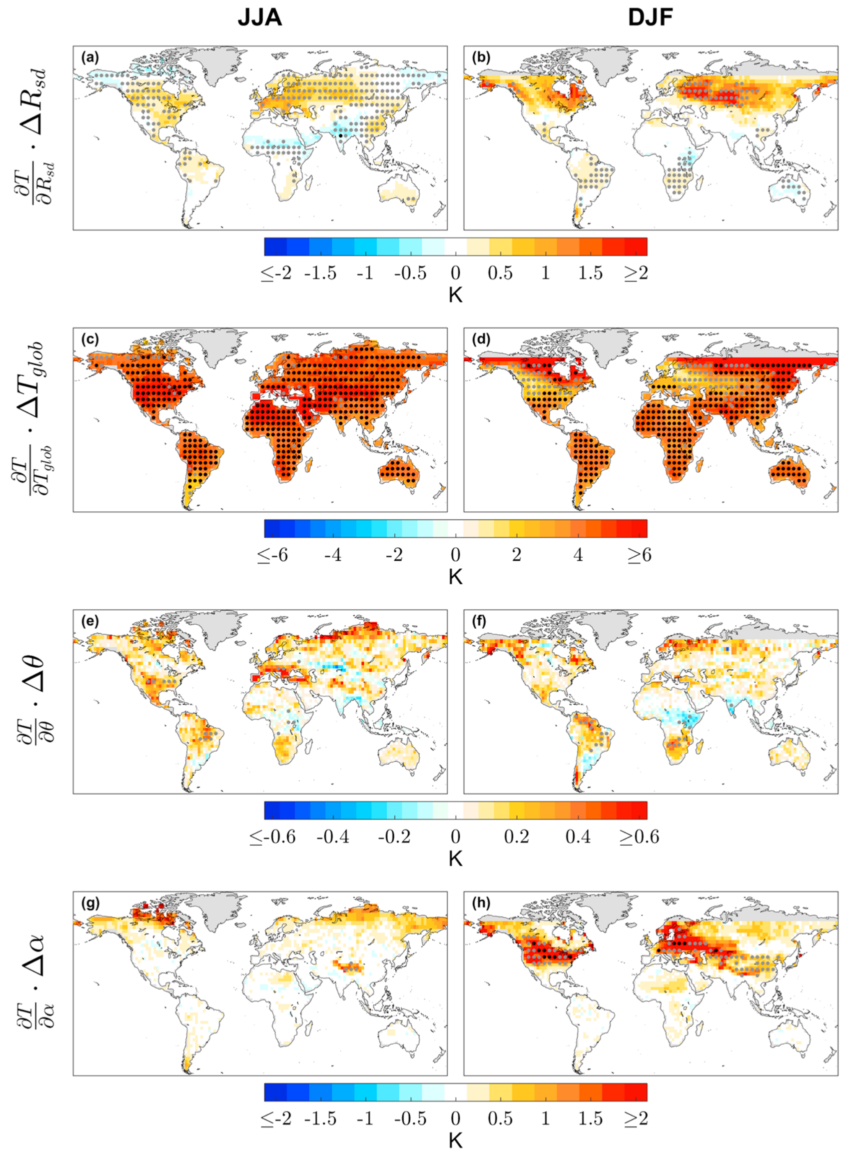

Figure 4. As in Figure 3 (right columns), that is, for the multidecadal temperature trend 1970–2099, but using global mean temperature T_{glob} instead of incoming longwave radiation as explanatory variable. Note the different colorbar limits.

4.2. Emerging Patterns

Both for interannual temperature variability and multidecadal temperature trend, the R^2 values are high in almost all regions of the world. Only for interannual variability, R^2 values are lower in some arid and semi-arid regions (Figures 2a and 2b), indicating that in these regions additional processes not considered here also contribute to interannual temperature variations.

The effect of incoming longwave radiation on temperature is especially strong in high northern latitudes during winter, both for interannual variability and multidecadal trend (Figures 3e–3h). This effect can be explained by clouds that hinder thermal radiation to leave to space and keep temperatures high, while (nighttime) clear-sky conditions cause temperatures to decrease. Although shortwave radiation is also impacted by cloud cover, its influence in high latitudes during winter is relatively low because of the flat incident angles and the low energy (Figures 3a–3d). In other regions, the impact of shortwave radiation on the multidecadal temperature trend is strongly connected to changes in cloud cover (see supporting information Figure S7). The projected decrease of cloud cover in large parts of the world during summer leads to higher incoming shortwave radiation and, thus, a positive contribution to the temperature trend. The widespread increase of cloud cover in North America and Eurasia during winter causes a reduction of incoming shortwave radiation and, thus, a negative impact on the temperature trend (Figures 3c and 3d).

Soil moisture and near-surface air temperature are generally negatively coupled (Figures 1e and 1f, and S1e and S1f). The coupling direction can be identified by the relation between evapotranspiration and near-surface air temperature (see, e.g., Zscheischler et al., 2015): negative correlations indicate soil moisture control on temperature, and positive correlations point to atmospheric control on soil moisture. The correlations between evapotranspiration and temperature (supporting information Figure S8) indicate that most of the regions where soil moisture and temperature are strongly coupled (see Figures 3i–3l) are soil moisture controlled. Only some areas in rainforests reveal atmospheric control on soil moisture. On the multidecadal time scale, projected decreases of soil moisture (supporting information Figure S7) cause a warming of near-surface air in several regions (Figures 3k and 3l).

The importance of albedo is highest in regions that experience varying snow cover in different years or snow cover changes with climate change (Figures 3m–3p). In some arid and semi-arid regions (e.g., Sahara and Sahel), albedo and temperature are positively related, which is very likely due to some sporadic rain events after which the soil is darker and temperatures are lower. The albedo signal in the Amazon region might be caused by land cover changes due to deforestation. Considering the multidecadal trend, global warming leads to a poleward shift of the areas in which snow cover affects near-surface air temperature, resulting in positive albedo impacts on temperature in high northern latitudes during JJA as well as North America and Eurasia during DJF.

4.3. Robustness of Results and Limits of Multiple Linear Regression

The results presented here are based on the output of 35 CMIP5 models. To test their robustness, we applied the same analysis to the reanalysis products ERA-Interim and ERA-Interim/Land (Balsamo et al., 2015; Dee et al., 2011), which should be less model dependent for variables that undergo an assimilation of observations. The results (supporting information Figures S9–S11) are very similar (although more noisy) to those obtained from the climate models, indicating that the climate model-based results are robust. Additionally, the results for interannual temperature variability are consistent when using a 50-year time period (1970–2019) instead. Moreover, all results are consistent when applying LASSO regression instead of stepwise MLR. The uncertainty of R^2 estimated by jackknife resampling for the stepwise MLR is on average lower than 0.02 (interquartile range), both for interannual temperature variability and multidecadal trend.

Since many processes in the Earth System are nonlinear (Good et al., 2015), using a linear regression model is a simplification of reality. Still it is a helpful tool to estimate first-order contributions, even if it does not allow to draw any conclusions about causal relations. While for some processes causality based on the physical understanding of the Earth System can be established, feedbacks within the system can also reverse this causality. Moreover, inherent collinearities between the different explanatory variables make it hard to estimate the relative importance of the single driving mechanisms for temperature variability and trend. Thus, we use the method proposed by Azen and Budescu (2003) that tries to consider these collinearities to calculate the contributions of the single explanatory variables.

As many other studies, we use a limited set of explanatory variables as input for our linear model. Thus, (hidden) variables that are not considered in the analysis, but have (potential) control on some of the considered variables, can affect the results. Examples of such variables are thermal advection, heat entrainment, cloud cover, greenhouse gas and water vapor concentrations in the atmosphere, land cover change, precipitation, and evapotranspiration. It is, however, not the aim of this study to perform a comprehensive analysis of all possible drivers but to limit the analysis to a set of variables that we consider as key for assessing the radiative and land surface contributions to interannual temperature variability and multidecadal temperature trend.

5. Conclusions

The present study investigates the impact of incoming shortwave radiation, incoming longwave radiation, soil moisture, and albedo on the interannual variability and multidecadal trend of monthly means of daily maximum near-surface air temperature using stepwise multiple linear regression. The four considered variables can explain 79% of interannual temperature variability and 99% of multidecadal temperature trend on land (Figures 2a and 2b and supporting information Figures S2a and S2b). While radiation is an essential variable over almost all land area, land surface conditions have a pronounced impact on temperature variability and trend in some confined regions (Figures 1, 2c–2f, supporting information Figures S1 and S2). This is also reflected in the effect that typical variations of the explanatory variables have on interannual temperature variability (Figure 3, left columns). Splitting the multidecadal temperature trend into its different contributions (Figure 3, right columns) reveals that incoming longwave radiation contributes homogeneously to the warming trend, while the effect of incoming shortwave radiation, soil moisture, and albedo exhibits more spatial variations and is opposing the trend in some regions.

Overall, for interannual temperature variability the radiation components contribute about 0.60 to total R^2, while the land components (soil moisture and albedo) account for about 0.20. For the multidecadal temperature trend, radiation contributes about 0.85, and the land surface 0.15 to total R^2. Although for both interannual variability and multidecadal trend radiation contributes a higher fraction to the explained variances, for the high explanatory power of the linear model both radiation and land surface processes are essential.

Acknowledgments
We thank Diego G. Miralles and an anonymous reviewer for the thorough review and valuable comments to our manuscript. We acknowledge the World Climate Research Programme's Working Group on Coupled Modelling, which is responsible for CMIP, and we thank the climate modeling groups (listed in supporting information Table S1) for producing and making available their model output. For CMIP the U.S. Department of Energy's Program for Climate Model Diagnosis and Intercomparison provides coordinating support and led development of software infrastructure in partnership with the Global Organization for Earth System Science Portals. CMIP5 data can be downloaded at https://esgf-node.llnl.gov/search/cmip5/. ERA-Interim and ERA-Interim/Land data can be obtained at http://apps.ecmwf.int/datasets/. The processed data can be downloaded from the ETH Research collection (doi:20.500.11850/221784). This study was supported by the European Research Council (ERC) "DROUGHT-HEAT" project funded through the European Community's Seventh Framework Programme (grant agreement FP7-IDEAS-ERC-617518).

References

Arrhenius, S. (1896). XXXI. On the influence of carbonic acid in the air upon the temperature of the ground. *The London, Edinburgh, and Dublin Philosophical Magazine and Journal of Science*, *41*(251), 237–276. https://doi.org/10.1080/14786449608620846

Azen, R., & Budescu, D. V. (2003). The dominance analysis approach for comparing predictors in multiple regression. *Psychological methods*, *8*(2), 129–148. https://doi.org/10.1037/1082-989X.8.2.129

Balsamo, G., Albergel, C., Beljaars, A., Boussetta, S., Brun, E., Cloke, H., et al. (2015). ERA-Interim/Land: A global land surface reanalysis data set. *Hydrology and Earth System Sciences*, *19*(1), 389–407. https://doi.org/10.5194/hess-19-389-2015

Berg, A., Sheffield, J., & Milly, P. C. (2017). Divergent surface and total soil moisture projections under global warming. *Geophysical Research Letters*, *44*, 236–244. https://doi.org/10.1002/2016GL071921

Brown, B. L., & Hendrix, S. B. (2005). *Encyclopedia of statistics in behavioral science, chap. Partial Correlation Coefficients*. Hoboken, NJ: John Wiley & Sons, Ltd. https://doi.org/10.1002/0470013192.bsa469

Budyko, M. I. (1969). The effect of solar radiation variations on the climate of the Earth. *Tellus*, *21*(5), 611–619. https://doi.org/10.1111/j.2153-3490.1969.tb00466.x

Chylek, P., Klett, J. D., Dubey, M. K., & Hengartner, N. (2016). The role of Atlantic Multi-decadal Oscillation in the global mean temperature variability. *Climate Dynamics*, *47*(9-10), 3271–3279. https://doi.org/10.1007/s00382-016-3025-7

Compo, G. P., & Sardeshmukh, P. D. (2009). Oceanic influences on recent continental warming. *Climate Dynamics*, *32*(2), 333–342. https://doi.org/10.1007/s00382-008-0448-9

Dee, D. P., Uppala, S. M., Simmons, A. J., Berrisford, P., Poli, P., Kobayashi, S., et al. (2011). The ERA-Interim reanalysis: Configuration and performance of the data assimilation system. *Quarterly Journal of the Royal Meteorological Society*, *137*(656), 553–597. https://doi.org/10.1002/qj.828

Efron, B. (1982). *The jackknife, the bootstrap, and other resampling plans* (Vol. 38). Philadelphia: Society for Industrial and Applied Mathematics.

Ellis, A. W., & Leathers, D. J. (1999). Analysis of cold airmass temperature modification across the US Great Plains as a consequence of snow depth and albedo. *Journal of Applied Meteorology*, *38*(6), 696–711. https://doi.org/10.1175/1520-0450(1999)038<0696:AOCATM>2.0.CO;2

Fischer, E., Rajczak, J., & Schär, C. (2012). Changes in European summer temperature variability revisited. *Geophysical Research Letters*, *39*, L19702. https://doi.org/10.1029/2012GL052730

Good, P., Lowe, J. A., Andrews, T., Wiltshire, A., Chadwick, R., Ridley, J. K., et al. (2015). Nonlinear regional warming with increasing CO_2 concentration. *Nature Climate Change*, *5*(2), 138–142. https://doi.org/10.1038/NCLIMATE2498

Graversen, R. G., & Wang, M. (2009). Polar amplification in a coupled climate model with locked albedo. *Climate Dynamics*, *33*(5), 629–643. https://doi.org/10.1007/s00382-009-0535-6

Hall, A. (2004). The role of surface albedo feedback in climate. *Journal of Climate*, *17*(7), 1550–1568. https://doi.org/10.1175/1520-0442(2004)017<1550:TROSAF>2.0.CO;2

Hocking, R. R. (1976). A biometrics invited paper. The analysis and selection of variables in linear regression. *Biometrics*, *32*(1), 1–49. https://doi.org/10.2307/2529336

Hoerling, M., Kumar, A., Eischeid, J., & Jha, B. (2008). What is causing the variability in global mean land temperature? *Geophysical Research Letters*, *35*, L23712. https://doi.org/10.1029/2008GL035984

Holmes, C. R., Woollings, T., Hawkins, E., & De Vries, H. (2016). Robust future changes in temperature variability under greenhouse gas forcing and the relationship with thermal advection. *Journal of Climate*, *29*(6), 2221–2236. https://doi.org/10.1175/JCLI-D-14-00735.1

Intergovernmental Panel on Climate Change (2013). *Climate Change 2013: The Physical Science Basis. Contribution of Working Group I to the Fifth Assessment Report of the Intergovernmental Panel on Climate Change* (pp. 1535). Cambridge United Kingdom and New York: Cambridge University Press. https://doi.org/10.1017/CBO9781107415324

Jaeger, E., & Seneviratne, S. (2011). Impact of soil moisture–atmosphere coupling on European climate extremes and trends in a regional climate model. *Climate Dynamics*, *36*(9), 1919–1939. https://doi.org/10.1007/s00382-010-0780-8

Ji, F., Wu, Z., Huang, J., & Chassignet, E. P. (2014). Evolution of land surface air temperature trend. *Nature Climate Change*, *4*(6), 462–466. https://doi.org/10.1038/NCLIMATE2223

Jones, D. (1999). Characteristics of Australian land surface temperature variability. *Theoretical and Applied Climatology*, *63*(1-2), 11–31. https://doi.org/10.1007/s007040050088

Jones, P., Lister, D., Osborn, T., Harpham, C., Salmon, M., & Morice, C. (2012). Hemispheric and large-scale land-surface air temperature variations: An extensive revision and an update to 2010. *Journal of Geophysical Research*, *117*, D05127. https://doi.org/10.1029/2011JD017139

Koster, R. D., Guo, Z., Yang, R., Dirmeyer, P. A., Mitchell, K., & Puma, M. J. (2009). On the nature of soil moisture in land surface models. *Journal of Climate*, *22*(16), 4322–4335. https://doi.org/10.1175/2009JCLI2832.1

Legates, D. R., & Willmott, C. J. (1990). Mean seasonal and spatial variability in global surface air temperature. *Theoretical and Applied Climatology*, *41*(1), 11–21. https://doi.org/10.1007/BF00866198

Lenderink, G., Van Ulden, A., Van den Hurk, B., & Van Meijgaard, E. (2007). Summertime inter-annual temperature variability in an ensemble of regional model simulations: Analysis of the surface energy budget. *Climatic Change*, *81*, 233–247. https://doi.org/10.1007/s10584-006-9229-9

Lohmann, U., & Feichter, J. (2005). Global indirect aerosol effects: A review. *Atmospheric Chemistry and Physics*, *5*(3), 715–737. https://doi.org/10.5194/acp-5-715-2005

Miralles, D., Berg, M. v., Teuling, A., & Jeu, R. d. (2012). Soil moisture-temperature coupling: A multiscale observational analysis. *Geophysical Research Letters*, *39*, L21707. https://doi.org/10.1029/2012GL053703

Miralles, D. G., Teuling, A. J., van Heerwaarden, C. C., & de Arellano, J. V.-G. (2014). Mega-heatwave temperatures due to combined soil desiccation and atmospheric heat accumulation. *Nature Geoscience*, *7*(5), 345–349. https://doi.org/10.1038/ngeo2141

Neter, J., Nachtsheim, C. J., & Kutner, M. H. (2004). *Applied linear regression models* (4th ed.). Maidenhead: McGraw Hill.

Orth, R., & Seneviratne, S. I. (2017). Variability of soil moisture and sea surface temperatures similarly important for warm-season land climate in the Community Earth System Model. *Journal of Climate*, *30*(6), 2141–2162. https://doi.org/10.1175/JCLI-D-15-0567.1

Philipona, R., Dürr, B., Ohmura, A., & Ruckstuhl, C. (2005). Anthropogenic greenhouse forcing and strong water vapor feedback increase temperature in Europe. *Geophysical Research Letters*, *32*, L19809. https://doi.org/10.1029/2005GL023624

Pithan, F., & Mauritsen, T. (2014). Arctic amplification dominated by temperature feedbacks in contemporary climate models. *Nature Geoscience*, *7*(3), 181–184. https://doi.org/10.1038/NGEO2071

Reitan, C. H. (1974). A climatic model of solar radiation and temperature change. *Quaternary Research*, *4*(1), 25–38. https://doi.org/10.1016/0033-5894(74)90061-1

Riahi, K., Rao, S., Krey, V., Cho, C., Chirkov, V., Fischer, G., et al. (2011). RCP 8.5—A scenario of comparatively high greenhouse gas emissions. *Climatic Change*, *109*(1-2), 33. https://doi.org/10.1007/s10584-011-0149-y

Rodrigues, R. R., & Woollings, T. (2017). Impact of atmospheric blocking on South America in austral summer. *Journal of Climate*, *30*(5), 1821–1837. https://doi.org/10.1175/JCLI-D-16-0493.1

Scherrer, S. C., Appenzeller, C., Liniger, M. A., & Schär, C. (2005). European temperature distribution changes in observations and climate change scenarios. *Geophysical Research Letters*, *32*, L19705. https://doi.org/10.1029/2005GL024108

Schleussner, C.-F., Runge, J., Lehmann, J., & Levermann, A. (2014). The role of the North Atlantic overturning and deep ocean for multi-decadal global-mean-temperature variability. *Earth System Dynamics*, *5*(1), 103–115. https://doi.org/10.5194/esd-5-103-2014

Schwingshackl, C., Hirschi, M., & Seneviratne, S. I. (2017). Quantifying spatiotemporal variations of soil moisture control on surface energy balance and near-surface air temperature. *Journal of Climate*, *30*(18), 7105–7124. https://doi.org/10.1175/JCLI-D-16-0727.1

Seneviratne, S. I., Corti, T., Davin, E. L., Hirschi, M., Jaeger, E. B., Lehner, I., et al. (2010). Investigating soil moisture–climate interactions in a changing climate: A review. *Earth-Science Reviews*, *99*(3), 125–161. https://doi.org/10.1016/j.earscirev.2010.02.004

Seneviratne, S. I., Donat, M. G., Pitman, A. J., Knutti, R., & Wilby, R. L. (2016). Allowable CO_2 emissions based on regional and impact-related climate targets. *Nature*, *529*(7587), 477–483. https://doi.org/10.1038/nature16542

Seneviratne, S. I., Lüthi, D., Litschi, M., & Schär, C. (2006). Land–atmosphere coupling and climate change in Europe. *Nature*, *443*(7108), 205–209. https://doi.org/10.1038/nature05095

Sillmann, J., & Croci-Maspoli, M. (2009). Present and future atmospheric blocking and its impact on European mean and extreme climate. *Geophysical Research Letters*, *36*, L10702. https://doi.org/10.1029/2009GL038259

Stephens, G. L., & Webster, P. J. (1981). Clouds and climate: Sensitivity of simple systems. *Journal of the Atmospheric Sciences*, *38*(2), 235–247. https://doi.org/10.1175/1520-0469(1981)038<0235:CACSOS>2.0.CO;2

Stolpe, M. B., Medhaug, I., & Knutti, R. (2017). Contribution of atlantic and pacific multidecadal variability to twentieth-century temperature changes. *Journal of Climate*, *30*(16), 6279–6295. https://doi.org/10.1175/JCLI-D-16-0803.1

Sutton, R., Suckling, E., & Hawkins, E. (2015). What does global mean temperature tell us about local climate? *Philosophical Transactions of the Royal Society A*, *373*(2054). https://doi.org/10.1098/rsta.2014.0426

Taylor, K. E., Stouffer, R. J., & Meehl, G. A. (2012). An overview of CMIP5 and the experiment design. *Bulletin of the American Meteorological Society*, *93*(4), 485–498. https://doi.org/10.1175/BAMS-D-11-00094.1

Tibshirani, R. (1996). Regression shrinkage and selection via the LASSO. *Journal of the Royal Statistical Society. Series B (Methodological)*, *58*(1), 267–288.

Velicer, W. F. (1978). Suppressor variables and the semipartial correlation coefficient. *Educational and Psychological Measurement*, *38*(4), 953–958. https://doi.org/10.1177/001316447803800415

Wilks, D. S. (2016). “The stippling shows statistically significant gridpoints”: How research results are routinely overstated and overinterpreted, and what to do about it. *Bulletin of the American Meteorological Society*, *97*(12), 2263–2273. https://doi.org/10.1175/BAMS-D-15-00267.1

Xoplaki, E., Gonzalez-Rouco, J., Luterbacher, J., & Wanner, H. (2003). Mediterranean summer air temperature variability and its connection to the large-scale atmospheric circulation and SSTs. *Climate Dynamics*, *20*(7-8), 723–739. https://doi.org/10.1007/s00382-003-0304-x

Zscheischler, J., Orth, R., & Seneviratne, S. I. (2015). A submonthly database for detecting changes in vegetation-atmosphere coupling. *Geophysical Research Letters*, *42*, 9816–9824. https://doi.org/10.1002/2015GL066563